

Microscopic growth mechanism and edge states ofmonolayer 1T'-$MoTe_2$

Haipeng Zhao(赵海鹏), Yin Liu(刘隐), Shengguo Yang(杨胜国), Chenfang Lin(林陈昉), Mingxing Chen(陈明星), Kai Braun, Xinyi Luo(罗心仪), Siyu Li(李思宇), Anlian Pan(潘安练), and Xiao Wang(王笑)

Citation: Chin. Phys. B, 2024, 33 (**4**): 046801. DOI: 10.1088/1674-1056/ad16d5
Journal homepage: http://cpb.iphy.ac.cn; http://iopscience.iop.org/cpb

What follows is a list of articles you may be interested in

Growth and characterization of Bi(110)/$CrTe_2$ heterostructures: Exploring interplay between magnetism and topology

Zhenyu Yuan(袁震宇), Fazhi Yang(杨发枝), Baiqing Lv(吕佰晴), Yaobo Huang(黄耀波), Tian Qian(钱天), Jinpeng Xu(徐金朋), and Hong Ding(丁洪)

Chin. Phys. B, 2024, 33 (**2**): 026802. DOI: 10.1088/1674-1056/ad082a

Adsorption structure of macrocyclic energetic molecule DOATF on Au(111)

Xiao Chang(常霄), Li Huang(黄立), Yixuan Gao(高艺璇), Changjiang Yu(于长江), Yun Cao(曹云), Long Lv(吕龙), Xiao Lin(林晓), Shixuan Du(杜世萱), and Hong-Jun Gao(高鸿钧)

Chin. Phys. B, 2023, 32 (**9**): 096802. DOI: 10.1088/1674-1056/acda84

Manipulating charge density wave state in kagome compound RbV_3Sb_5

Yu-Xin Meng(孟雨欣), Cheng-Long Xue(薛成龙), Li-Guo Dou(窦立国), Wei-Min Zhao(赵伟民), Qi-Wei Wang(汪琪玮), Yong-Jie Xu(徐永杰), Xiangqi Liu(刘祥麒), Wei Xia(夏威), Yanfeng Guo(郭艳峰), and Shao-Chun Li(李绍春)

Chin. Phys. B, 2023, 32 (**9**): 096801. DOI: 10.1088/1674-1056/acd8b1

Critical behavior in the epitaxial growth of two-dimensional tellurium films on $SrTiO_3$ (001) substrates

Haimin Zhang(张海民), Dezhi Song(宋德志), Fuyang Huang(黄扶旸), Jun Zhang(仉君), and Ye-Ping Jiang(蒋烨平)

Chin. Phys. B, 2023, 32 (**6**): 066802. DOI: 10.1088/1674-1056/acc80d

Visualizing interface states in In_2Se_3–WSe_2 monolayer lateral heterostructures

Da Huo(霍达), Yusong Bai(白玉松), Xiaoyu Lin(林笑宇), Jinghao Deng(邓京昊), Zemin Pan(潘泽敏), Chao Zhu(朱超), Chuansheng Liu(刘传胜), and Chendong Zhang(张晨栋)

Chin. Phys. B, 2023, 32 (**5**): 056803. DOI: 10.1088/1674-1056/acbaef

---

Microscopic growth mechanism and edge states of monolayer 1T′-$MoTe_2$

Haipeng Zhao(赵海鹏)[1], Yin Liu(刘隐)[1], Shengguo Yang(杨胜国)[2,3], Chenfang Lin(林陈昉)[1], Mingxing Chen(陈明星)[2,3], Kai Braun[4], Xinyi Luo(罗心仪)[1], Siyu Li(李思宇)[1], Anlian Pan(潘安练)[1,†], and Xiao Wang(王笑)[1,‡]

[1] *Key Laboratory for Micro-Nano Physics and Technology of Hunan Province, School of Physics and Electronics, College of Materials Science and Engineering, Hunan University, Changsha* 410082, *China*

[2] *Key Laboratory of Low-Dimensional Quantum Structures and Quantum Control of Ministry of Education, Synergetic Innovation Centre for Quantum Effects and Applications (SICQEA), Hunan Normal University, Changsha* 410081, *China*

[3] *State Key Laboratory of Powder Metallurgy, Central South University, Changsha* 410083, *China*

[4] *Institute of Physical and Theoretical Chemistry and LISA+, University of Tübingen, Auf der Morgenstelle 18*, 72076 *Tübingen, Germany*

(Received 4 November 2023; revised manuscript received 11 December 2023; accepted manuscript online 19 December 2023)

Transition metal ditellurides (TMTDs) have versatile physical properties, including non-trivial topology, Weyl semimetal states and unique spin texture. Controlled growth of high-quality and large-scale monolayer TMTDs with preferred crystal phases is crucial for their applications. Here, we demonstrate the epitaxial growth of 1T′-$MoTe_2$ on Au (111) and graphitized silicon carbide (Gr/SiC) by molecular beam epitaxy (MBE). We investigate the morphology of the grown 1T′-$MoTe_2$ at the atomic level by scanning tunnelling microscopy (STM) and reveal the corresponding microscopic growth mechanism. It is found that the unique ordered Te structures preferentially deposited on Au (111) regulate the growth of monolayer single crystal 1T′-$MoTe_2$, while the Mo clusters were preferentially deposited on the Gr/SiC substrate, which impedes the ordered growth of monolayer $MoTe_2$. We confirm that the size of single crystal 1T′-$MoTe_2$ grown on Au (111) is nearly two orders of magnitude larger than that on Gr/SiC. By scanning tunnelling spectroscopy (STS), we observe that the STS spectrum of the monolayer 1T′-$MoTe_2$ nano-island at the edge is different from that at the interior, which exhibits enhanced conductivity.

Keywords: transition metal ditellurides, 1T′-$MoTe_2$, microscopic growth mechanism, scanning tunneling microscopy/spectroscopy (STM/S)

PACS: 68.37.Ef, 73.20.–r, 37.20.+j **DOI:** 10.1088/1674-1056/ad16d5

1. Introduction

Group VI transition metal ditellurides (TMDTs) materials of MTe_2 (M represents a transition-metal atom of Mo, W, and Cr) have drawn extensive attention owing to their multifunctionality in novel physical properties derived from the diversity of phases (e.g., 1H, 1T, and 1T′).[1–8] The 1H phase is a direct band gap semiconductor, which has a broad application prospect in the field of optoelectronics;[9,10] while the 1T phase prone to phase transition to form a metastable 1T′ phase that originates from the lateral deformation of metal atoms of the 1T structures, creating a zigzag chain due to Peierls distortion.[11,12] The 1T and 1T′ phases exhibit exotic physical properties such as anisotropic spin–orbit coupling,[13] Weyl semimetal (WSM) states,[1,3,4] superconductivity,[1,4] and quantum spin Hall states (QSHSs).[5,6,8] Among the TMDTs families, 1T′-$MoTe_2$ is a representative TMDTs material, which has been demonstrated as a semimetal with superconductivity,[4] and has been predicted to be a Weyl semimetal[3] in bulk materials and a topological insulator in monolayer.[6] Recently, ultrathin 1T′-$MoTe_2$ has been characterized by concurrent in-plane and out-of-plane spin polarizations, forming a new spin Hall effect.[14]

To date, chemical vapor deposition (CVD)[15–18] and molecular-beam epitaxy (MBE)[19–21] are typical methods for the controlled growth of 1T′-$MoTe_2$. For CVD, the grown 1T′-$MoTe_2$ films usually have a relatively low crystalline quality and exhibit high contamination on the surface. For MBE, the 1T′-$MoTe_2$ film is usually grown on graphitized silicon carbide (Gr/SiC).[22] The grown film has different crystallographic orientations within a small area (about 10 nm) and shows a mixture of 1H and 1T′ phases due to the small energy difference ($\Delta E < 0.05$ eV) between these two phases.[23] Hence, on the one hand, it is essential to find a more appropriate substrate to grow large-scale monolayer 1T′-$MoTe_2$ single crystals. Recently, Au (111) has been reported as a substrate for the growth of transition metal dichalcogenides (TMDCs),[24,25] demonstrating the potential for the unidirectionally oriented growth. On the other hand, understanding the 1T′-$MoTe_2$ growth mechanism at the atomic level is crucial, which can provide fundamental insights into the growth of single crystals.

Here we present the controllable epitaxial growth of 1T′-

†Corresponding author. E-mail: anlian.pan@hnu.edu.cn
‡Corresponding author. E-mail: xiao_wang@hnu.edu.cn

© 2024 Chinese Physical Society and IOP Publishing Ltd

$MoTe_2$ monolayers on Au (111) and Gr/SiC by MBE. Based on our scanning tunnelling microscopy/spectroscopy (STM/S) measurements, we demonstrate that the deposited unique ordered Te structures (labelled as V-structures) on Au (111) regulate the growth of large-scale monolayer 1T′-$MoTe_2$ single crystal with lengths beyond 1 μm; while Mo nucleation sites on Gr/SiC substrate impede the growth, leading to small monolayers of $MoTe_2$ with the size of about 10 nm. In addition, via STS measurements, we observe that the edge of monolayer 1T′-$MoTe_2$ has enhanced conductivity.

2. Methods

In sample preparations and STM/STS measurements, the experiments were conducted in an ultrahigh vacuum (UHV) scanning tunneling microscopy (STM) system (Unisoku 1400LT) consisting of a preparation chamber for molecular beam epitaxy (MBE) and an observation chamber for STM investigations. Both chambers had a base pressure of 2×10^{-10} torr. The preparation chamber was equipped with a Knudsen effusion cell for tellurium (99.999%), and an e-beam evaporator for molybdenum (99.95%). The Gr/SiC substrates were prepared by vacuum annealing. The Au (111) single crystal was cleaned by repeated cycles of Ar^+ sputtering (1.6 keV), followed by annealing at 630 °C until no contamination could be detected by STM. The growth time was 10 min if no special instruction is given. The STM investigations were carried out by home-build tungsten tips. STM imaging and STS measurements were performed at 77 K. The dI/dV spectra were obtained by a standard lock-in amplifier with a modulation frequency of 771 Hz and a modulation voltage of 10 mV.

The 1T′-$MoTe_2$ on Au (111) were characterized using scanning electron microscopy (SEM, ZEISS. Sigma HD), and Raman measurements were conducted using a confocal microscope (WITec, alpha-300) with an objective-focused 532 nm laser in the room temperature.

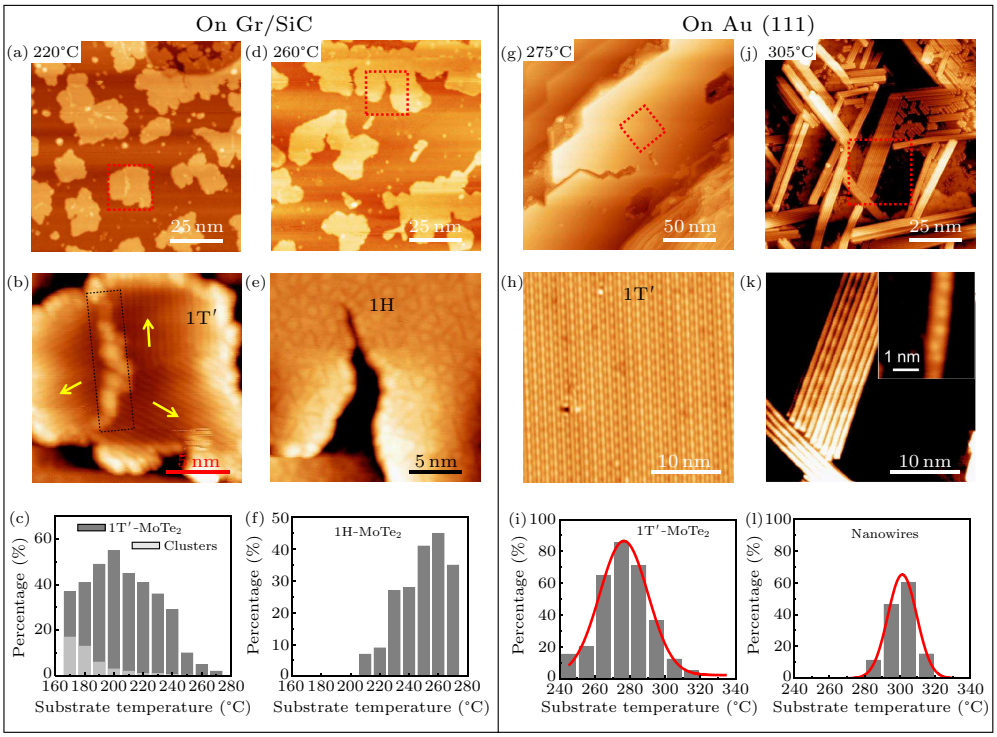


Fig. 1. Temperature-controlled growth of $MoTe_2$ on Gr/SiC and Au (111). (a) Large scale, (b) magnified STM images of 1T′-$MoTe_2$ grown on Gr/SiC at 220 °C. The yellow arrows and the black dashed rectangle mark the crystal orientation of 1T′-$MoTe_2$ and the cluster, respectively. (c) Proportion of 1T′-$MoTe_2$ and clusters grown on Gr/SiC as a function of substrate temperature. (d) Large scale, (e) magnified STM images of reconstructed 1H-$MoTe_2$ on Gr/SiC at 260 °C. (f) Proportion of 1H-$MoTe_2$ grown on Gr/SiC as a function of substrate temperature. (g) Large scale, (h) magnified STM images of 1T′-$MoTe_2$ on Au (111) at 275 °C. (i) Proportion of 1T′-$MoTe_2$ grown on Au (111) as a function of substrate temperature. (j) Large scale, (k) magnified STM images of Mo_6Te_6 nanowires grown on Au (111) at 305 °C. The upper right inset shows the STM image of a single Mo_6Te_6 nanowire. (l) Proportion of Mo_6Te_6 nanowires grown on Au (111) as a function of substrate temperature.

3. Results and discussion

We first grew $MoTe_2$ by MBE method on Gr/SiC with substrate temperature ranging from 170 to 320 °C (the default growth time is 10 min, and the ratio of Te to Mo is 30 to 1), and performed STM measurements on the samples (see Fig. S1 in supporting information). Figures 1(a), 1(b) and 1(d), 1(e) show STM images of $MoTe_2$ monolayers grown at two typical temperatures. According to the atomically resolved structures from STM images, we can conclude that the 1T′-$MoTe_2$ islands tend to form at a lower substrate temperature, e.g., 220 °C [Figs. 1(a) and 1(b)]. Noticeably, the magnified STM image [Fig. 1(b)] shows the 1T′-$MoTe_2$ island has different

crystal orientations (shown by the yellow arrows) and small clusters (marked by black dashed rectangle), which are mainly considered as Mo clusters according to later detailed analysis. In contrast, the 1H-$MoTe_2$ islands are dominant at a higher substrate temperature, e.g., 260 °C [Figs. 1(d) and 1(e)], exhibiting the reconstruction structures and the clean surface, which is in line with previous reports on the MBE growth of $MoTe_2$.[19,20] We also recorded STS spectra from the two samples (see Fig. S2 in supporting information), confirming the formation of 1T′-$MoTe_2$ and 1H-$MoTe_2$. Statistical analysis on the crystallinity of the samples grown at different substrate temperatures [Figs. 1(c) and 1(f)] indicates that the metastable 1T′-$MoTe_2$ gradually changes to stable 1H-$MoTe_2$ with an increasing temperature of the substrate. For instance, when substrate temperature increases from 220 °C to 260 °C, the percentage of 1T′-$MoTe_2$ decreases from 41% to 5%, while the percentage of 1H-$MoTe_2$ increases from 9% to 44%. Meanwhile, the clusters become smaller and even disappear as the substrate temperature increases [Fig. 1(c)]. When the substrate temperature rises to about 320 °C, one-dimensional nanowires emerge (see Fig. S1 in supporting information), similar to prior reported 1D Mo_6Te_6 nanowires.[21,26] From the above experimental results, we conclude that only small-size single-crystal 1T′-$MoTe_2$ can be realized on Gr/SiC substrate.

In contrast, we performed a series of MBE growths of $MoTe_2$ on Au (111) substrate with the temperature ranging from 245 °C to 335 °C (the default growth time is 10 min, and the ratio of Te to Mo is 20 to 1). We find that the dominant products are Te films, 1T′-$MoTe_2$, nanowires, and clusters with increasing substrate temperature (see Fig. S3 in supporting information). At 275 °C, the grown monolayer single crystal 1T′-$MoTe_2$ almost covers the entire Au (111) facet [Fig. 1(g)] and the high-resolution STM image [Fig. 1(h)] shows a high-quality single crystal 1T′-$MoTe_2$. Increasing the Au (111) temperature to 305 °C, we observe straight nanowires with a length of more than 60 nm [Figs. 1(j) and 1(k)], which are determined as Mo_6Te_6 with further STM and STS investigations (see Fig. S4 in supporting information). Figures 1(i) and 1(l) show the crystallinity percentage of 1T′-$MoTe_2$ and nanowires as a function of substrate temperature, which satisfies the Gaussian fitting (red curves), indicating that the substrate temperature greatly influences the growth process.

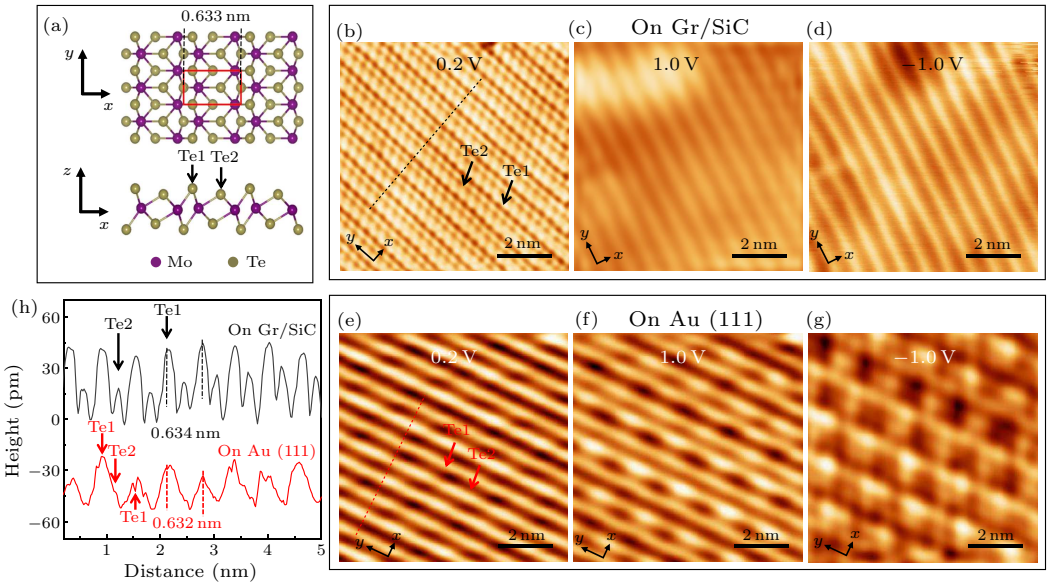


Fig. 2. Atomic structural analysis of 1T′-$MoTe_2$ by STM on Gr/SiC and Au (111). (a) Schematic of the lattice structure of 1T′-$MoTe_2$ viewing from the top (top panel) and side (bottom panel). The unit cell is marked by the red rectangle. Te1 and Te2 represent two adjacent Te atoms along the x axis, respectively. (b)–(g) Atomic-resolved STM images at different bias voltages of 1T′-$MoTe_2$ on Gr/SiC substrate [(b)–(d)] and Au (111) substrate [(e)–(g)]. The value of bias voltage is marked in the images. (h) The height line profile collected along the dashed black line and dashed red line in (b) and (e), respectively.

Atomic structures of 1T′-$MoTe_2$ grown on Gr/SiC and Au (111) can be clearly resolved by STM imaging. The schematic model of the 1T′-$MoTe_2$ [Fig. 2(a)] shows the zigzag chain along the y axis, resulting in the adjacent Te atoms in the x direction (Te1 and Te2) are not on the same plane. Figure 2(b) shows the atomic resolution STM image of 1T′-$MoTe_2$ grown on Gr/SiC at low bias (0.2 V), and all Te atoms on the upper surface can be clearly resolved. STM probes the local density of state (LDOS) on the sample surface, which is determined by the sample surface real height information and the electronic state information. Therefore, different substrates and different scanning bias voltages affect the STM topography of the grown sample. For the STM images recorded at higher biases (1 V and −1 V) [Figs. 2(c) and 2(d)], due to the influence of the electronic state, the slight height fluctuation of the adjacent Te atoms in the y direction is not dominant. In

contrast, the apparent height difference of adjacent Te atoms (Te1 and Te2) in the x direction is easier to detect, so the images show light and dark stripes. For the 1T′-$MoTe_2$ grown on Au (111), the STM image recorded at 0.2 V shows light and dark stripes [Fig. 2(e)] rather than atomically resolved patterns shown in Fig. 2(b), which indicates that the interaction of electronic state between Au (111) and 1T′-$MoTe_2$ is very strong even at a low bias (0.2 V). Further, STM images at higher bias (1 V and −1 V) show moiré patterns induced from 1T′-$MoTe_2$ and the substrate Au (111) [Figs. 2(f) and 2(g)]. This also suggests a strong electronic interaction between them. Figure 2(h) shows the height line profiles collected along the black and red dashed lines in Figs. 2(b) and 2(e). The lattice constants of 1T′-$MoTe_2$ grown on Gr/SiC and Au (111) are 0.634 nm and 0.632 nm, respectively, which is consistent with the theoretical lattice constant of 1T′-$MoTe_2$ of 0.633 nm.[27] Significantly, due to the influence of Au (111), the appearance of Te2 is much less obvious than that on Gr/SiC.

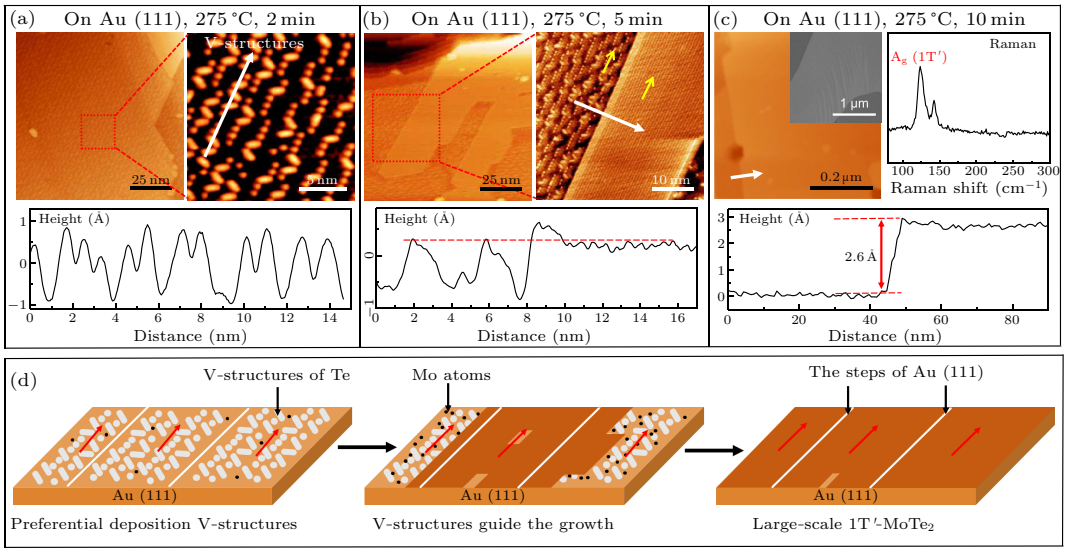


Fig. 3. The evolution process of V-structures induced growth of large-scale1T′-$MoTe_2$ on Au (111). (a) Large-scale magnified STM images (the top panel) of the ordered Te-structures (V-structures). The height line profile (the bottom panel) was collected along the white arrow, and the height of the V-structures is about 1.6 Å. The growth time is 2 min. (b) Large-scale magnified STM images (the top panel) of 1T′-$MoTe_2$ edge. The two yellow arrows indicate that 1T′-$MoTe_2$ and the V-structures are in the same orientation. The height line profile (the bottom panel) was collected along the white arrow, spanning 1T′-$MoTe_2$ and V-structures. The growth time is 5 min. (c) The STM image of single crystals 1T′-$MoTe_2$ at the submicron level (in the left panel), and the inset is the SEM image of 1T′-$MoTe_2$. The right panel shows the Raman spectroscopy of 1T′-$MoTe_2$, and a distinct Raman mode near 125 cm^{-1}, corresponding to the A_g mode of 1T′-$MoTe_2$. The height line profile (the bottom panel) was collected along the white arrow in the left panel, and the height is about 2.6 Å, indicating the single atomic step of Au (111). The growth time is 10 min. (d) Schematic illustration of the 1T′-$MoTe_2$ growth process on Au (111).

To understand the growth mechanism of 1T′-$MoTe_2$ on Au (111) substrate, it is critical to regulate the growth time under the suitable growth conditions and clarify the characteristics of the growth process. Hence, we performed a comparative analysis of the grown samples with different growth times at 275 °C. The left panel of Fig. 3(a) is an STM image with a growth time of 2 min, from which it can be clearly observed that the surface of Au (111) is covered with a layer of ordered structures with the height of about 1.6 Å [the bottom panel of Fig. 3(a)]. The local detail magnification [the right panel of Fig. 3(a)] shows that the ordered structures are very similar to the previously reported Te structures.[28] To verify whether these are Te structures, we deposited Te on Au (111) alone for 2 min, and we observed the same structures (see Fig. S5 in supporting information). Since the local pattern of the Te structures is V-shaped, we label them as V-structures. In addition, the orientation of V-structures on a single facet surface of Au (111) was consistent and it can also be consistent on multiple facets (see Fig. S5 in supporting information). This indicates that the Au (111) surface determines the growth orientation of the V-structures.

To investigate whether the V-structures can effectively regulate the growth of 1T′-$MoTe_2$, the epitaxial growth is carried out on Au (111) for 5 min. We found that the V-structures still exist outside the edge of the 1T′-$MoTe_2$ [the left panel of Fig. 3(b)], but with some adsorbed atoms [the right panel of Fig. 3(b)] compared to the V-structures shown in Fig. 3(a). Moreover, the formed 1T′-$MoTe_2$ and V-structures have the same orientation [the yellow arrows in Fig. 3(b)], and the height difference between these two structures is extremely small [the bottom panel of Fig. 3(b)]. Based on the analysis, we conclude that V-structures guide the growth of 1T′-$MoTe_2$. We also strengthened this conclusion by comparing the STM images presented by another sample at different growth times (see Fig. S6 in supporting information). In addition, we performed normal epitaxial growth of 1T′-$MoTe_2$ on the Au (111) substrate with Te clusters (see Fig. S7 in supporting informa-

tion), and obtained clusters instead of 1T′-$MoTe_2$. This further indicates that the V-structures are critical to the growth of 1T′-$MoTe_2$.

The large-scale STM image of single crystal 1T′-$MoTe_2$ on a single Au (111) facet with 10 min growth time is shown in the left panel of Fig. 3(c). Its size reaches the submicron level, which is nearly two orders of magnitude larger than the size of 1T′-$MoTe_2$ grown by MBE in previous reports.[19,20,29] In addition, the scanning electron microscope (SEM) image [inset of the left panel of Fig. 3(c)] shows that 1T′-$MoTe_2$ can grow across Au (111) steps. The height profile [the bottom panel of Fig. 3(c)] shows that the height of the steps is 2.6 Å, which is consistent with the thickness of a single layer Au (111). This indicates that 1T′-$MoTe_2$ is uniformly covered on the Au (111) surface. The more information of the 1T′-$MoTe_2$ single crystal is shown in Fig. S8 of in supporting information. Furthermore, the samples are analyzed by Raman spectroscopy [the right panel of Fig. 3(c)], which exhibit a distinct Raman mode near 125 cm^{-1}, corresponding to the A_g mode of 1T′-$MoTe_2$.[30]

The schematic illustration of the 1T′-$MoTe_2$ growth process on Au (111) is proposed in Fig. 3(d) based on the analysis of the above experimental conclusions. First, Te atoms are easily deposited on Au (111) to form the V-structures, and then the V-structures further reacts with Mo and Te to form 1T′-$MoTe_2$. As the reaction progresses, 1T′-$MoTe_2$ gradually grows and finally covers the whole Au (111) surface.

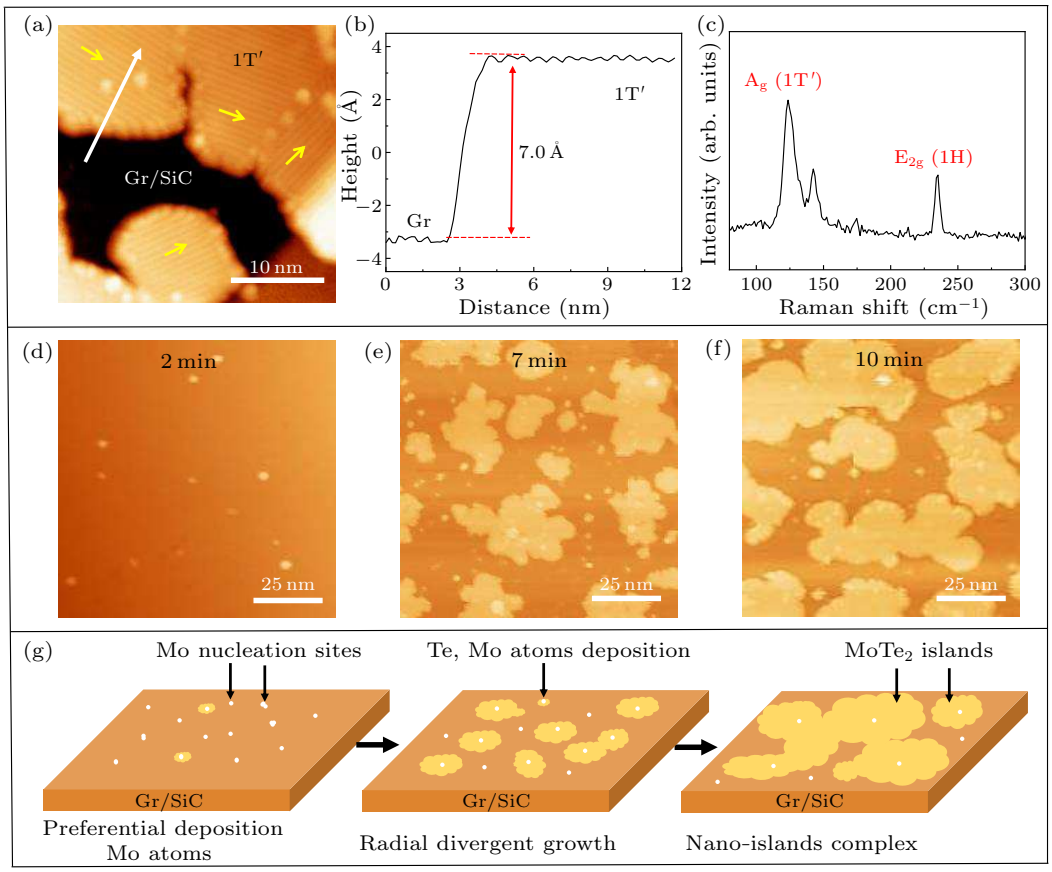


Fig. 4. Microscopic growth mechanism of $MoTe_2$ on Gr/SiC. (a) STM image of 1T′-$MoTe_2$ grown at 240 °C. The yellow arrows mark the different orientations of 1T′-$MoTe_2$. (b) The height line profile of 1T′-$MoTe_2$. The line is collected along the white arrow in (a), and the height of the 1T′-$MoTe_2$ is about 7 Å. (c) The Raman spectroscopy of $MoTe_2$ on Gr/SiC. There are two distinct Raman modes near 125 cm^{-1} and 235 cm^{-1}, corresponding to the A_g mode of 1T′-$MoTe_2$ and the E_{2g} mode of 1H-$MoTe_2$, respectively. (d)–(f) STM images during the growth evolution of $MoTe_2$ with time: (d) 2 min, (e) 5 min, (f) 10 min. (g) Schematic illustration of the $MoTe_2$ growth process on Gr/SiC.

To elucidate the growth mechanism for 1T′-$MoTe_2$ on Gr/SiC, we first analyze the STM measurements for the best quality samples obtained under optimal growth conditions (growth temperature at 240 °C, growth time 10 min, and the flux ratio of Te and Mo being 30 to 1). We observed small 1T′-$MoTe_2$ nano-islands dominate [Fig. 4(a)] and with different crystal orientations. This is in stark contrast to the large-scale single crystal 1T′-$MoTe_2$ grown on Au (111). The STM height profile [Fig. 4(b)] shows that a height difference of 7 Å between the $MoTe_2$ nano-island and the substrate, indicating the formation of monolayer 1T′-$MoTe_2$.[19] The flux ratio of Te and Mo is 30 to 1, but the excessive Te atoms cannot be deposited on the blank Gr/SiC, reflecting the weak binding ability of Te and Gr/SiC substrate, which is also confirmed by our DFT calculations (see Fig. S10 in supporting information). Therefore, we consider that Te atoms are not dominant in the growth of $MoTe_2$ on Gr/SiC. The Raman spectroscopy [Fig. 4(c)] shows two distinct Raman modes near 125 cm^{-1}

and 235 cm^{-1}, corresponding to the A_g mode of 1T′-$MoTe_2$ and the E_{2g} mode of 1H-$MoTe_2$, respectively, which further illustrates that $MoTe_2$ grown on Gr/SiC is a mixture of two phases within the scale of the conventionally optical resolution.

To investigate how the Mo atoms affect the growth of 1T′-$MoTe_2$, we performed the time-controlled growth process. Figures 4(d)–4(f) show the STM images of samples grown on Gr/SiC at 240 °C for 2 min, 5 min, and 10 min, respectively. When the growth time was 2 min, nucleation sites were found on Gr/SiC [Fig. 4(d)]. Through comparative experiments of depositing Te atoms and simultaneously depositing both Te and Mo atoms (normal epitaxial growth method) on Gr/SiC with Mo clusters (see Fig. S9 in supporting information). We found that pure Te atoms cannot be deposited on Gr/SiC substrates with Mo clusters, while the normal epitaxial growth of $MoTe_2$ can be carried out using Mo clusters as nucleation sites. This indicates that these nucleation sites in Fig. 4(d) are mainly composed of Mo atoms. As the growth time increases, Te and Mo atoms start to gather and react around the Mo nucleation sites, and gradually epitaxially grow into small $MoTe_2$ nano-islands [Fig. 4(e)]. As the reaction proceeds further, the adjacent small nano-islands continue to expand and eventually grow together to form large nano-islands [Fig. 4(f)]. Since the crystal orientation of epitaxially grown 1T′-$MoTe_2$ at different Mo nucleation sites is random, the crystal orientation of the finally formed large nano-island on Gr/SiC substrate is diverse [Fig. 4(a)], as the results shown in the previous reports.[19,20] The relative growth evolution of $MoTe_2$ on Gr/SiC substrates is illustrated in Fig. 4(g).

We further performed STS measurements to investigate the energy band information of the grown 1T′-$MoTe_2$. Figures 5(a) and 5(c) show the STM images of typical monolayer 1T′-$MoTe_2$ grown on Gr/SiC and on Au (111), respectively. For both samples, we observed different dI/dV spectra at the edge and interior areas (referring to the bulk) [Figs. 5(b) and 5(d)]. We can clearly see the difference of the dI/dV spectra at the edge and bulk. The LDOS intensity at the edge is significantly enhanced, forming clear edge states. In general, the dI/dV spectrum at the edge shows a V-shaped spectrum, while the one in the bulk is flatter. This indicates that the 1T′-$MoTe_2$ has conductive edge states. Notably, due to the strong interaction between the Au (111) and 1T′-$MoTe_2$, the dI/dV spectra can be easily influenced by the electronic states of the Au (111), leading to that the intrinsic properties of 1T′-$MoTe_2$ is not obvious. In contrast, the dI/dV spectrum recorded from monolayer on Gr/SiC shows a clear zero-band gap at the edge with a V-shaped spectral profile, while the U-shaped dI/dV spectrum with an opened band gap appears at the bulk $MoTe_2$ [Fig. 5(b)]. Our observation agrees with the previously reported transport experiment[7] of 1T′-$MoTe_2$, which shows a bandgap opening of up to 60 meV, demonstrating that the monolayer 1T′-$MoTe_2$ has conductive edge states. We also performed dI/dV mapping on 1T′-$MoTe_2$ island grown on Gr/SiC at different bias voltages (see Fig. S11 in supporting information), finding that the length of the enhanced conductivity edge states is about 2 nm. This physical property of monolayer 1T′-$MoTe_2$ is similar to the characteristics of two-dimensional topological insulators, which have conductive edge states and insulating bulk states.[31–33]

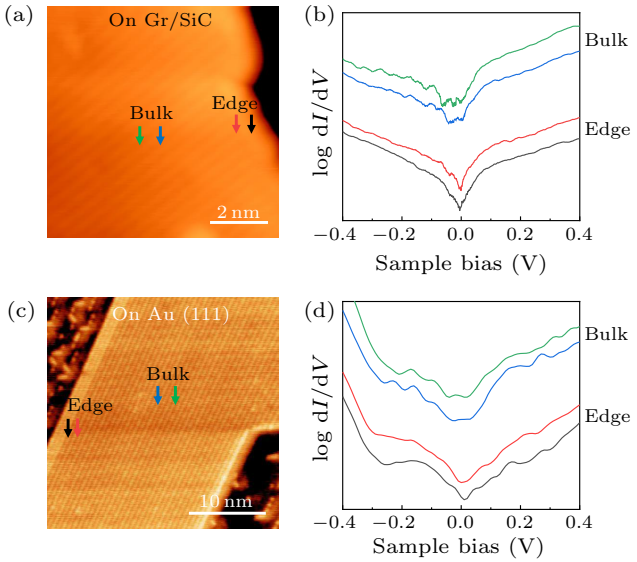


Fig. 5. STM/STS study of the edge states of 1T′-$MoTe_2$. (a) STM image of 1T′-$MoTe_2$ on Gr/SiC. (b) The dI/dV spectra collected at the locations marked by arrows in (a). (c) STM image of 1T′-$MoTe_2$ on Au (111). (d) dI/dV spectra collected at the locations marked by arrows in (c).

4. Conclusion and perspectives

We have performed epitaxial growth of $MoTe_2$ on Gr/SiC and Au (111) at different substrate temperatures and growth time by MBE method. By atomically resolved STM imaging, we systemically investigated the morphology and the crystal phase of the grown samples, revealing the microscopic mechanism of the growth of $MoTe_2$. We find that, even at the optimized substrate temperature, only small size single 1T′-$MoTe_2$ can be realized on Gr/SiC. This is due to the fact that the formed Mo nucleation sites on substrate impede the further growth of monolayer $MoTe_2$. For Au (111) substrate, we found that the firstly formed Te structures (V-structures) regulate and promote the growth of monolayer single crystal 1T′-$MoTe_2$, leading to nearly two orders of magnitude larger crystal size compared to that grown on the Gr/SiC. By STS measurements, we demonstrate that the monolayer 1T′-$MoTe_2$ has conductive edge states. Our study not only provides the fundamental understanding of microscopic growth mechanism of 1T′-$MoTe_2$, but also experimentally verifies that it has conductive edge states, which could pave the way for device applications based on 1T′-$MoTe_2$.

Acknowledgments

Project supported by the National Key R&D Program of China (Grant No. 2022YFA1204302), the National Natural Science Foundation of China (Grant Nos. 52022029, 52221001, 92263107, U23A20570, 62090035, U19A2090, and 12174098), the Hunan Provincial Natural Science Foundation of China (Grant Nos. 2022JJ30142 and 2019XK2001), and in part supported by the State Key Laboratory of Powder Metallurgy, Central South University. Calculations were carried out using computing resources at the High Performance Computing Platform of Hunan Normal University.

References

[1] Wang W, Kim S, Liu M, Cevallos F, Cava R and Ong N 2020 *Science* **368** 534
[2] Soluyanov A A, Gresch D, Wang Z, Wu Q, Troyer M, Dai X and Bernevig B 2015 *Nature* **527** 495
[3] Wang Z, Gresch D, Soluyanov A A, Xie W, Kushwaha S, Dai X, Troyer M, Cava R J and Bernevig B A 2016 *Phys. Rev. Lett.* **117** 056805
[4] Qi Y, Naumov P G, Ali M N, Rajamathi C R, Schnelle W, Barkalov O, Hanfland M, Wu S C, Shekhar C, Sun Y, Suss V, Schmidt M, Schwarz U, Pippel E, Werner P, Hillebrand R, Forster T, Kampert E, Parkin S, Cava R J, Felser C, Yan B and Medvedev S A 2016 *Nat. Commun.* **7** 11038
[5] Tang S, Zhang C, Wong D, Pedramrazi Z, Tsai H Z, Jia C, Moritz B, Claassen M, Ryu H, Kahn S, Jiang J, Yan H, Hashimoto M, Lu D, Moore R G, Hwang C C, Hwang C, Hussain Z, Chen Y, Ugeda M M, Liu Z, Xie X, Devereaux T P, Crommie M F, Mo S K and Shen Z X 2017 *Nat. Phys* **13** 683
[6] Qian X, Liu J, Fu L and Li J 2014 *Science* **346** 1344
[7] Keum D H, Cho S, Kim J H, Choe D H, Sung H J, Kan M, Kang H, Hwang J Y, Kim S W, Yang H, Chang K J and Lee Y H 2015 *Nat. Phys.* **11** 482
[8] Chen P, Pai W W, Chan Y H, Sun W L, Xu C Z, Lin D S, Chou M Y, Fedorov A V and Chiang T C 2018 *Nat. Commun.* **9** 2003
[9] Zhu Y, Li Z, Zhang L, Wang B, Luo Z, Long J, Yang J, Fu L and Lu Y 2018 *ACS Appl. Mater. Interfaces* **10** 43291
[10] Chen W, Liang R, Wang J, Zhang S and Xu J 2018 *Sci. Bull.* **63** 997
[11] Whangbo M H and Canadell E 1992 *J. Am. Chem. Soc.* **114** 9587
[12] Heising J and Kanatzidis M 1999 *J. Am. Chem. Soc.* **121** 638
[13] Cui J, Li P, Zhou J, He W Y, Huang X, Yi J, Fan J, Ji Z, Jing X, Qu F, Cheng Z G, Yang C, Lu L, Suenaga K, Liu J, Law K T, Lin J, Liu Z and Liu 2019 *Nat. Commun.* **10** 2044
[14] Vila M, Hsu C H, Garcia J H, Benítez L A, Waintal X, Valenzuela S O, Pereira V M and Roche S 2021 *Phys. Rev. Res.* **3** 043230
[15] Guo Z, Wang L, Han M, Zhao E, Zhu L, Guo W, Tan J, Liu B, Chen X Q and Lin J 2022 *ACS Nano* **16** 11268
[16] Pace S, Martini L, Convertino D, Keum D H, Forti S, Pezzini S, Fabbri F, Miseikis V and Coletti C 2021 *ACS Nano* **15** 4213
[17] Yang L, Zhang W, Li J, Cheng S, Xie Z and Chang H 2017 *ACS Nano* **11** 1964
[18] Zhou L, Zubair A, Wang Z, Zhang X, Ouyang F, Xu K, Fang W, Ueno K, Li J, Palacios T, Kong J and Dresselhaus M S 2016 *Adv. Mater.* **28** 9526
[19] Chen J, Wang G, Tang Y, Tian H, Xu J, Dai X, Xu H, Jia J, Ho W and Xie M 2017 *ACS Nano* **11** 3282
[20] Yu Y, Wang G, Tan Y, Wu N, Zhang X A and Qin S 2018 *Nano Lett.* **18** 675
[21] Li Y, Wu D, Wang D, Zhang Y, Min T and Pan Y 2022 *Adv. Mater. Interfaces* **10** 2202043
[22] Wang Q, Zhang W, Wang L, He K, Ma X and Xue Q 2013 *J. Phys.: Condens. Matter* **25** 095002
[23] Duerloo K A, Li Y and Reed E J 2014 *Nat. Commun.* **5** 4214
[24] Cheng F, Hu Z, Xu H, Shao Y, Su J, Chen Z, Ji W and Loh K P 2019 *ACS Nano* **13** 2316
[25] Yang P, Wang D, Zhao X, Quan W, Jiang Q, Li X, Tang B, Hu J, Zhu L, Pan S, Shi Y, Huan Y, Cui F, Qiao S, Chen Q, Liu Z, Zou X and Zhang Y 2022 *Nat. Commun.* **13** 3238
[26] Zhu H, Wang Q, Zhang C, Addou R, Cho K, Wallace R M and Kim M J 2017 *Adv. Mater.* **29** 1606264
[27] Dawson W and Bullett D 1987 *J. Phys. Chem. C* **20** 6159
[28] Guan J, Huang X, Xu X, Zhang S, Jia X, Zhu X, Wang W and Guo 2018 *Surf. Sci.* **669** 198
[29] Pham T T, Castelino R, Felten A and Sporken R 2020 *Appl. Surf. Sci.* **523** 146428
[30] Cho S, Kim S, Kim J H, Zhao J, Seok J, Keum D H, Baik J, Choe D H, Chang K J and Suenaga K 2015 *Science* **349** 625
[31] Bernevig B A and Zhang S C 2006 *Phys. Rev. Lett.* **96** 106802
[32] Kane C L and Mele E J 2005 *Phys. Rev. Lett.* **95** 226801
[33] Konig M, Wiedmann S, Brune C, Roth A, Buhmann H, Molenkamp L W, Qi X L and Zhang S C 2007 *Science* **318** 766